Radiocarbon (2025), pp. 1–17
doi:10.1017/RDC.2025.10143

CAMBRIDGE UNIVERSITY PRESS

RESEARCH ARTICLE

Holocene effusive flank eruptions in Masaya caldera, Nicaragua

Denis-Ramón Avellán[1], Martha Gabriela Gómez-Vasconcelos[2] and Martín Pilato[3]

[1]SECIHTI- Instituto de Geofísica, Universidad Nacional Autónoma de México, UNAM Campus Morelia, Michoacán, México, [2]SECIHTI- Instituto de Investigaciones en Ciencias de la Tierra, Universidad Michoacana de San Nicolás de Hidalgo, Morelia, Michoacán, México and [3]Calibre Mining Corp, Residencial Las Colinas no. 273, Managua, Nicaragua
Corresponding author: Denis-Ramón Avellán; Email: davellan@igeofisica.unam.mx

Received: 21 November 2024; **Revised:** 08 August 2025; **Accepted:** 09 August 2025

Keywords: basaltic caldera; flank eruption; Masaya caldera; Nicaragua; radiocarbon AMS dating

Abstract

Five unknown Holocene flank eruptions from the Masaya caldera are reported here. These eruptions comprise basaltic lava flows emplaced in Masaya's northern rift zone along the Cofradía fault zone, east of Managua City. The lava flows were defined as Mosintepe, Portillo, Gorgonia, Campuzano, and Martha units. Paleosol samples were collected below each lava flow, and radiocarbon AMS analyses were performed, yielding ages of 2250 ± 30, 1610 ± 30, 1600 ± 30, 1140 ± 30, and 790 ± 30 yrs BP, respectively. Calibrated age intervals are 285–229 cal BC for Mosintepe, 496–534 cal AD for Portillo, 496–535 cal AD for Gorgonia, 914–976 cal AD for Campuzano, and 1226–1268 cal AD for Martha; all stratigraphically consistent. These eruptions emitted magma bulk volumes between 0.02 and 0.51 km^3, reaching up to 8 km from their eruptive vent and 13 km from Masaya's polygenetic system summit crater. Their mineral paragenesis, and major and trace element geochemical fingerprint reveals a common volcanic provenance from the Masaya caldera due to lateral magma draining. This study demonstrates that basaltic lava flow flank eruptions are common in the Masaya caldera along its northern volcanic rift zone. Therefore, this information should be considered in future hazard and risk assessments.

Introduction

Flank eruptions in basaltic calderas are mainly caused by lateral magma draining from a common shallow magma chamber (Moore 1992). Most of these eruptions are effusive; however, they might be succeeded by caldera collapse, magma draining, or explosive eruptions (e.g., Kaneko et al. 2005; Simkin and Howard 1970). Therefore, determining if these eruptions are linked to the central caldera (summit conduit) or not (peripheral dike intrusion) is crucial for a better understanding of basaltic calderas and their hazard assessment.

Flank eruptions may be fed by sub-horizontal or radial dikes from a central conduit, likely related to local compressional stresses or aligned along preexisting tectonic structures (i.e., Acocella and Neri 2003). Volcanic rift zones represent preferred magma pathways because of their extensional component (crustal weakness zones; Gudmundsson and Loetveit 2005). For instance, most eruptions in the Kilauea and Mauna Loa basaltic calderas originate at the rift zones, and areas downhill of rift zones are more likely to be covered by future lava flows (Patrick et al. 2020).

The Masaya caldera complex is a dominantly effusive 11 × 6 km-diameter basaltic caldera that belongs to the central portion of the Nicaraguan Volcanic Arc, located in the SE Managua Graben (Figure 1) (Avellán et al. 2012; La Femina et al. 2002; Girard and van Wyk de Vries 2005). Masaya is currently unrest in a post-caldera phase; it has an active lava lake that occupies one of the summit craters (Santiago) and emits continuous gasses (Global Volcanism Program 2024). Over a dozen intra-caldera vents have sourced eruptions, and pit craters have formed due to magma draining (Harris 2009; Rymer

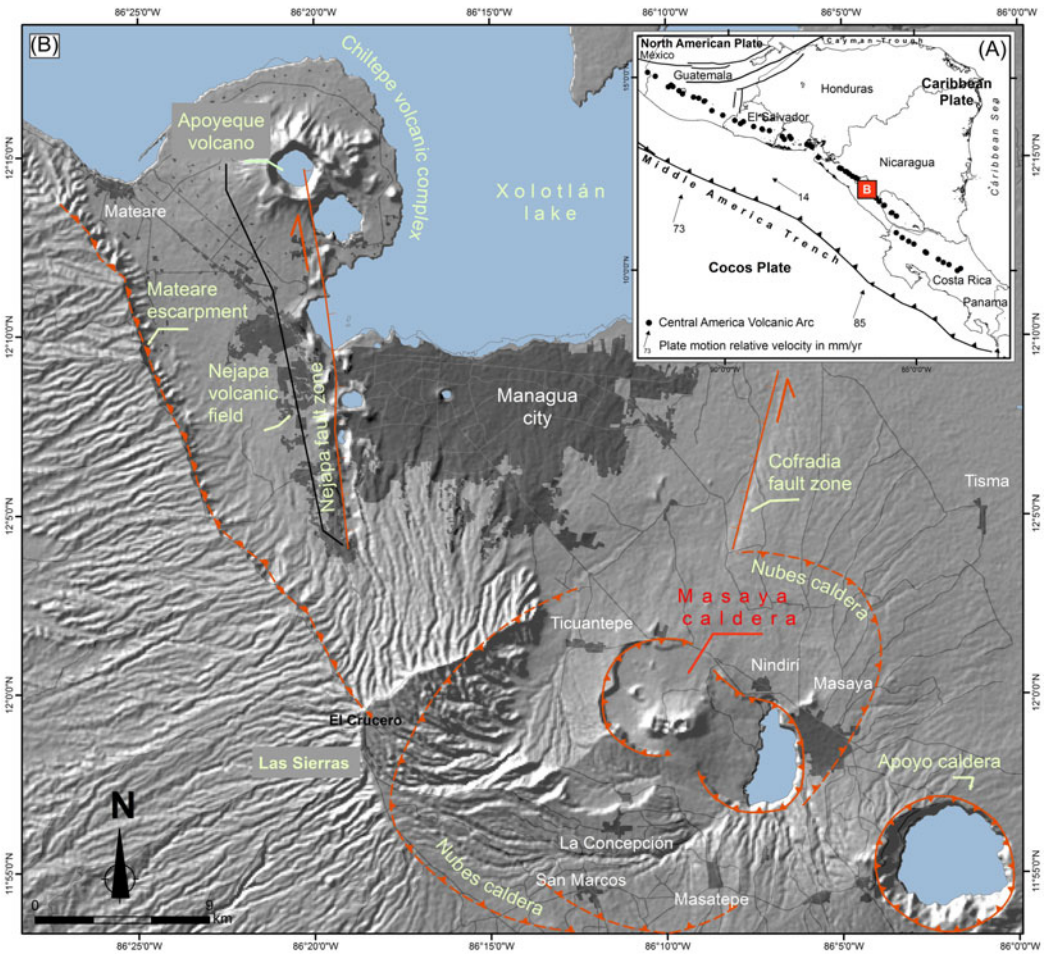

Figure 1. *The tectonic setting of the Masaya caldera in the Nicaraguan Volcanic Arc (A), its location, and main volcanic and tectonic structures (B). Projected coordinate system NAD 1927 UTM 16N.*

et al. 1998). Historic eruptions since 1529 CE are mainly associated with the Masaya-Nindirí vents (Fernández de Oviedo 1851) and have impacted the nearest localities, including Managua, Nicaragua's capital city. The last two eruptions happened in 1670 and 1772 CE; the former flowed down the northern slope related to an overflow of the Nindirí lava lake, and the latter took place from a fissure on the northern flank of Masaya cone (McBirney 1956).

Many recent lava flows in the northern flank of the Masaya caldera remain unstudied. Determining the age of these eruptions and their relation to Masaya's post-caldera activity is essential to complete the geological record for a better hazard assessment. Therefore, this work focuses on five effusive eruptions in the northern slopes of the Masaya caldera. The products were studied via geological mapping, radiocarbon dating, and geochemical analyses to determine their radiometric age and volcanic provenance. This allowed to identify new Masaya's flank eruptions.

Methods

To determine the age of five flank eruptions from the Masaya caldera, the distribution of each lava flow unit was mapped to ensure that the collected samples were obtained directly from the paleosols buried by each event. The mapping comprised tracing the geological contacts and analyzing the

https://doi.org/10.1017/RDC.2025.10143 Published online by Cambridge University Press

geomorphological chronology of the eruptions aided by satellite images obtained from the Basemap tool in ArcMap® 10.2 software. This helped us know the location of the eruptive vents and define the extension of each lava flow unit, considering the presence of vegetation, texture, and color contrast on the lava flow rocks. During the edition of the lithological contacts, the orthophotographs with a single band and pixel depth of 8 bit acquired from Instituto Nicaragüense de Estudios Territoriales were superimposed and referenced. 1988 images of the regional topographic map were used to corroborate some vectorial parameters. The map edition was georeferenced to the coordinate system GCS WGS 1984. After that, geological mapping was performed; it helped us defining each lava flow unit's distribution and stratigraphic position. This geological map also includes the two historical eruptions of 1670 and 1772 CE that occurred within the Masaya caldera.

After mapping, samples of paleosols were obtained directly from the paleosols buried by each event. Then, five samples of paleosols were collected. Three samples were collected from small manual pits made in front or on the edge of each lava flow unit emitted by different eruptive vents, while the other two samples were collected from excavation quarries. All samples were taken within 5 cm of the upper paleosol, below and in direct contact with each lava flow deposit. 10 g was sent to the laboratory to be analyzed by an accelerator mass spectrometry (AMS) at the Beta Analytic testing laboratory in Miami, Florida, USA. The standard methodology used in this laboratory is explained fully at Beta Analytic's (2025) website.

For this study, a total of seven new whole-rock analyses were carried out. Major and trace elements were determined in five rock samples from each of the lava flows identified on the northern flank of the Masaya caldera, and one rock sample for each of the historical eruptions that occurred within the Masaya caldera. All samples were normalized to an anhydrous base and plotted with the help of Igpet® software. Detection limit values for major elements are 0.01%, and ≤ 2 ppm for trace elements. The whole-rock concentrations were performed using the following package: Lithium Metaborate/Tetraborate Fusion—ICP and ICP-MS (Inductively Coupled Plasma emission Mass Spectrometry) to determine all major elements and some trace elements; also, 4B1-Total Digestion-ICP, and 4B-INAA (Instrumental Neutron Activation Analysis) techniques for other trace elements in Activation Laboratories LTD at Ancaster, Ontario, Canada (Actlabs 2025). We compare the geochemical data obtained from historical eruptions that occurred within the caldera with the lava flows that took place on Masaya's northern flank for correlation and using the geochemical data as fingerprinting tools. This helped us to understand the geochemical characteristics of the lava flow units and know the provenance of the magmas before they reached the surface.

Results

Lava flow units

Geological mapping helped identify five lava flows on the northern outer flank of the Masaya caldera's ring fault border (Figure 2). These represent fissure effusive eruptions located between 4.8 and 12.8 km from the active post-caldera pit craters known as Nindirí, Santiago, and Masaya (Figure 2). The Masaya's northern flank holds the Aeropuerto graben, and the five volcanic fissures are contained in this tectonic structure (Figure 2). Three of these units, defined here as Portillo (*Po*), Campuzano (*Ca*), and Martha (*Mt*), are aligned in the southeastern end of the graben along the Cofradía fault zone (Figure 2). The other two units, Mosintepe (*Mo*) and Gorgonia (*Go*), are placed in the central part of the graben (Figure 2). The two historical eruptions of 1670 (Upper Nindirí Unit) and 1772 (Upper Masaya Unit) CE were also identified in the Nindirí post-caldera pit crater rim and the northern flank of the Masaya post-caldera volcano, respectively (Figure 2). The 1772 CE lava flow fissure has an NNE direction, parallel to the Cofradía fault zone.

The volcanic landforms associated with the fissures (vents) of each lava flow are small spatter cones between 10 and 40 m high with basal diameters from 0.1 to 0.2 km. These spatter cones are formed by welded and agglutinated scoria fragments with massive facies. All the lava flows flowed northwards,

https://doi.org/10.1017/RDC.2025.10143 Published online by Cambridge University Press

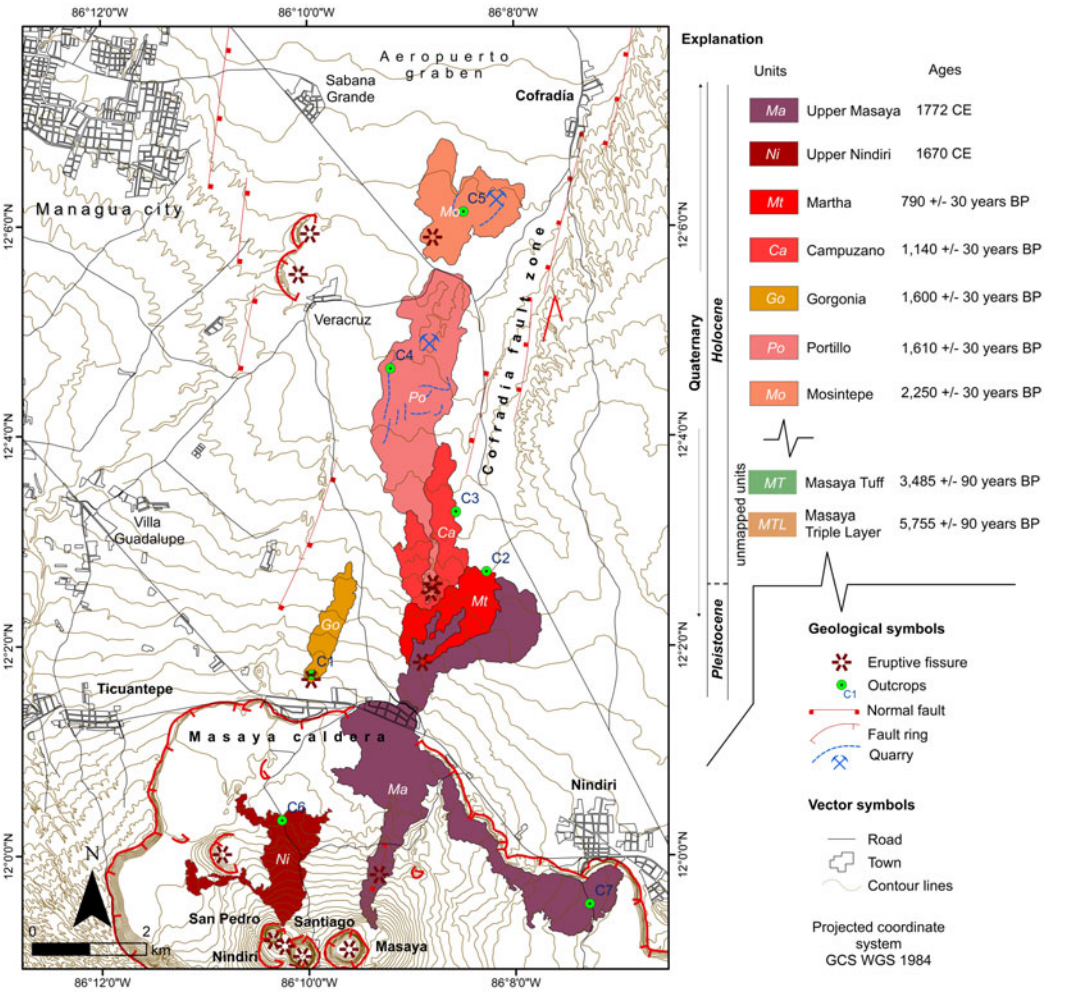

Figure 2. *Geological map of the Masaya caldera's northern portion, main eruptive fissures, and stratigraphic column for the studied volcanic units. The age of the Masaya Tuff (MT) Unit in the stratigraphic column was obtained from Avellán et al. (2012).*

reaching between 1.8 and 7.9 km (Table 1). They covered areas between 0.8 and 6.5 km^2, with bulk volumes from 0.02 to 0.51 km^3 (Table 1). All lava flow units present a massive structure with autobreccia facies in their border, top, and front portions. The rocks that make up these lava flows are formed by a gray groundmass and have a dominant fine-grained porphyritic texture with plagioclase (55–47 vol%), pyroxene (45–29 vol%), olivine (11–5 vol%), and Fe-Ti oxide (5–1.7 vol%) phenocrysts and microphenocrysts (Table 1).

Radiocarbon ages

The radiocarbon ages obtained by AMS from the collected paleosols were reported as conventional ^{14}C ages in years BP (Table 2) and accompanied by their values corresponding to $\delta^{13}C$, percent Modern Carbon, and $\Delta^{14}C$ (Table 2). These radiocarbon ages were calibrated to calendar years using the high probability density range method proposed by Ramsey (2009) through the IntCal20 terrestrial

https://doi.org/10.1017/RDC.2025.10143 Published online by Cambridge University Press

Table 1. *Main physical characteristics of the studied lava flow units.*

Unit	Vent location (UTM)		Eruption type	Lava flow length (km)	Lava flow area (km^2)	Lava flow volume (km^3)	Color of rock	Texture in hand sample	Mineralogical content (vol.%)	Phenocryst size (μm)	Matrix microlith size (μm)
	North	East									
Ma	1326349	591944	Central eruption	7.9	6.5	0.51	Dark	gray	Aphanitic	Pl, 53 > Px, 37 > Ol, 7 > Ox, 4	—
Pl,	20-1.8; Px, 9-1; Ox, 5-1.5; and Ol, 5-1										
Ni	1325333	590277	Central eruption	2.4	1.8	0.1	Gray	Fine-grained porphyritic, and glomeroporphyritic	Pl, 49 > Px, 40 > Ol, 6 > Ox, 5	Pl, 380-90; Px, 167-23; and Ol, 296-33	Pl, 33-3.3; Px, 16-1; Ol, 8.6-2; and Ox, 3.8-1.8
Mt	1330124	592706	Flank eruption	2	1.4	0.04	Gray	Fine-grained porphyritic, glomeroporphyritic	Pl, 47 > Px, 45 > Ol, 5 > Ox, 3	Pl, 292-62; Px, 153-50; and Ol, 80-28	Pl, 47-4; Px, 10-6 Ol, 10-2; and Ox, 9-1
Ca	1331506	592897	Flank eruption	2.5	1.8	0.07	Gray	Fine-grained porphyritic, seriate, glomeroporphyritic	Pl, 55 > Px, 29 > Ol, 11 > Ox, 5	Pl, 599-46; Px, 293-35; and Ol, 224-60	Pl, 13-1.7; Px, 9-1; Ol, 12-1; and Ox, 17-1.5
Go	1329823	590722	Flank eruption	2.2	0.8	0.04	Gray	Fine-grained porphyritic, glomeroporphyritic	Pl, 48 > Px, 44 > Ol, 6.3 > Ox, 1.7	Pl, 175-39; Px, 158-39; and Ol, 43-26	Pl, 33-5; Px, 12-2; Ol, 16-1; and Ox, 7-1.36
Po	1331331	592849	Flank eruption	5.7	4.6	0.09	Gray	Fine-grained porphyritic, seriate, glomeroporphyritic	Pl, 53 > Px, 40 > Ol, 5 > Ox, 2	Pl, 636-57; Px, 218-46; and Ol, 90-46	Pl, 22-4; Px, 10-1; Ol, 3-1; and Ox, 17-2
Mo	1337570	592881	Flank eruption	1.8	2.3	0.02	Gray	Fine-grained porphyritic, seriate, glomeroporphyritic	Pl, 49 > Px, 43 > Ol, 5 > Ox, 3	Pl, 526-154; Px, 89-49; and Ol, 111-40	Pl, 54-3; Px, 37-3; Ol, 35-1; and Ox, 17-1

Table 2. *Radiometric AMS ^{14}C ages results in years BP and calibrated to calendar dates BC and AD*

Field code	Location on the map		Lab code	Sample (stratigraphic unit)	^{14}C age (years BP)	$\delta^{13}C$ (‰)	pMC*	±	$\Delta^{14}C$ (‰)	±	Calibrated age 1σ	Confidence (68.2% probability)	Calibrated age 2σ	Confidence (95.4% probability)
	North	East												
C2	1331695	593831	619838	Paleosol below Martha lava flow (Mt)	790 ± 30	–20.4	90.63	0.34	–101.52	3.38	1226–1268 cal AD	68.20%	1214–1280 cal AD	95.40%
C3	1332738	593293	619842	Paleosol below Campuzano lava flow (Ca)	1140 ± 30	–19.5	86.77	0.32	–139.83	3.24	914–976 cal AD	52.20%	870–992 cal AD	82.20%
											883–902 cal AD	16%	827–862 cal AD	8.90%
													776–788 cal AD	4.30%
C1	1329824	590728	619837	Paleosol below Gorgonia lava flow (Go)	1600 ± 30	–16.2	81.94	0.31	–187.7	3.06	496–535 cal AD	32%	416–545 cal AD	95.40%
											449–478 cal AD	23.40%		
											425–441 cal AD	12.70%		
C4	1335252	592142	621921	Paleosol below Portillo lava flow (Po)	1610 ± 30	–25.3	81.84	0.31	–188.71	3.06	496–534 cal AD	31.40%	413–542 cal AD	95.40%
											455–478 cal AD	18.40%		
											418–440 cal AD	18.30%		
C5	1338011	593425	621920	Paleosol below Mosintepe lava flow (Mo)	2250 ± 30	–20	75.57	0.28	–250.84	2.82	285–229 cal BC	42.10%	315–204 cal BC	64.80%
											386–353 cal BC	26.10%	392–347 cal BC	30.60%

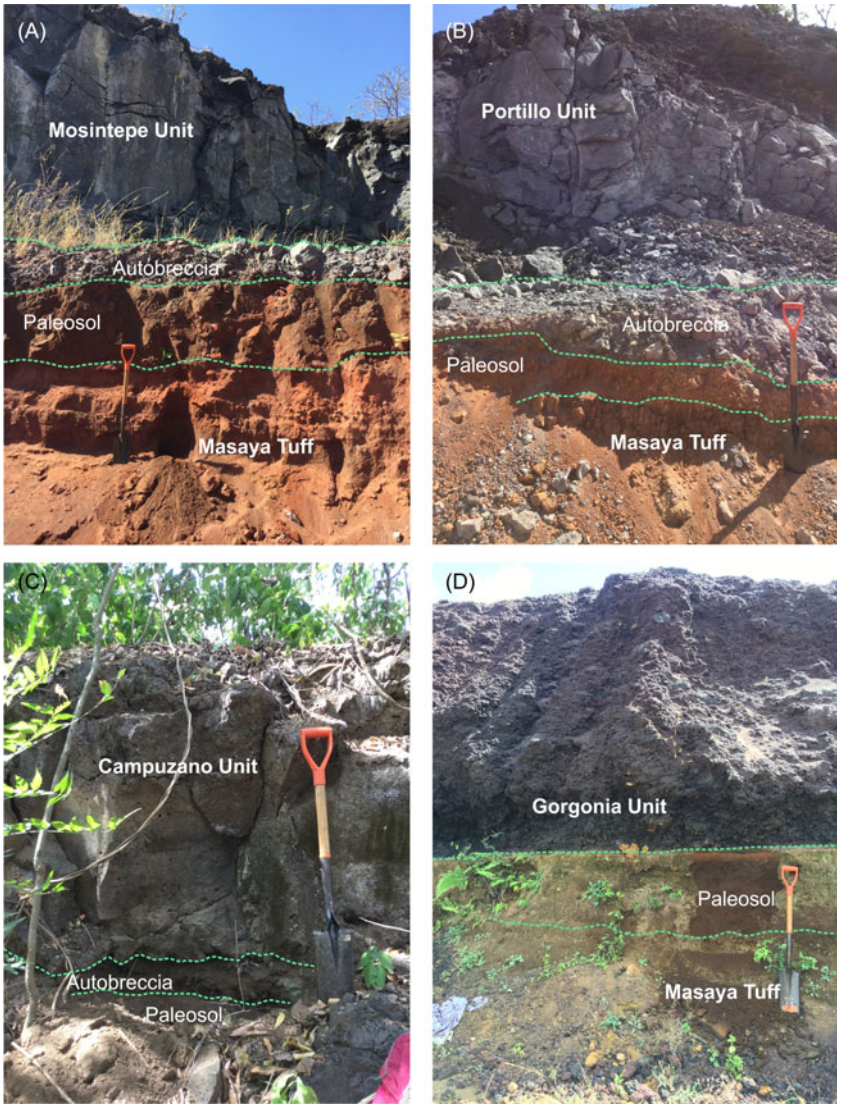

Figure 3. *Field outcrops of the Mosintepe, Portillo, Campuzano, and Gorgonia Units and their respective paleosols. The paleosols underlie the autobreccia facies, which form at the base of the lava flows.*

calibration curve of Reimer et al. (2020) for ^{14}C samples from the Northern Hemisphere. The calibrated age ranges calculated present values between 68.2% (1σ) and 95.4% (2σ) of probability (Table 2).

Two paleosol samples were collected at sites C4 and C5 (Figure 2) directly from the outcrops exposed in the quarries, corresponding to the *Mo* and *Po* Units (Figures 2, 3A, and 3B). These paleosols are reddish and are between 30 and 10 cm thick. They are reddish-brown, hardened, and have a massive structure with a clayey upper portion rich in hummus and a silty-sandy lower portion. These paleosols were developed from the deposit of the explosive eruption known as Masaya Tuff, which was recorded with an age of 3485 ± 90 yr BP (Avellán et al. 2012) and overlain by the lava flow units of *Mo* and *Po* (Figures 3A and 3B). Autobreccia facies of the lava flows in the lower portion trace the contact with the paleosols. The other three paleosol samples were collected at sites C1, C2, and C3 (Figures 2, 3C, and 3D) after excavating small pits with a shovel to expose the paleosols underlying the lava flow units *Go*,

https://doi.org/10.1017/RDC.2025.10143 Published online by Cambridge University Press

Ca, and *Mt*. These paleosols are up to 20 cm thick, dark brown, massive, slightly hardened, and enriched with black hummus and clayey silt. The eruption of 3.48 ka ago from the Masaya caldera is also underlying these paleosols, composed of gray tephra with lamellar structure, hardened and made up entirely of volcanic ash, recognized as a stratigraphic marker throughout the region.

AMS ^{14}C dating obtained from carbon disseminated within the paleosols collected at the base of the lava flows revealed radiometric ages of 2250 ± 30 years BP for *Mo* Unit, 1610 ± 30 years BP for *Po* Unit, 1600 ± 30 years BP for *Go* Unit, 1140 ± 30 years BP for *Ca* Unit, and 790 ± 30 years BP for *Mt* Unit (Table 2). They reveal $\Delta^{14}C$ values of –250.84 ± 2.82‰ for the *Mo* Unit, –188.71 ± 3.06‰ for the *Po* Unit, –187.7 ± 3.06‰ for the *Go* Unit, –139.83 ± 3.24‰ for the *Ca* Unit, and –101.52 ± 3.38‰ for the *Mt* Unit (Table 2).

Whole-rock composition

Almost all the lava flow rocks are of basaltic composition, except for the *Go* Unit, which is between the border of basaltic and basaltic andesite rocks (SiO_2 50.14–52 wt%) with MgO contents between 4.83 and 5.75 wt% (Table 3; Figures 4A and 4B). All the samples have sub-alkaline affinities and medium-K contents (Figure 4C).

Incompatible trace elements, graphed in a primitive mantle-normalized diagram, exhibit an identical pattern, revealing a relative enrichment in most incompatible elements (Cs, Rb, Ba, K, Pb, and Sr) in comparison with high field strength elements (Th, Nb, Zr, Ti, and Y) (Figure 4D). A multi-element rare earth graphic (Sun and McDonough 1989) points out that the rocks are slightly enriched in light rare earth elements in contrast to heavy rare earth elements (Figure 4E). All rocks display identical rare earth element concentrations without significant Eu anomalies (Figure 4D). Selected high-field strength trace elements reveal a homogeneous compositional group (Nb/Th-Ta/U) (Figure 4F).

Discussion

Radiocarbon geochronology

During an effusive eruption, the lava flows rapidly cover the soil. The thick lava flows aid in preserving the vertical paleosol profile, avoiding the migration of organic matter to lower horizons (Xu et al. 2013). Thus, radiometric AMS ^{14}C ages obtained from the disseminated charcoal within the paleosol's top portion covered by a lava flow represent the closest eruption age. This has been performed in several Holocene lava flows, which have been successfully dated with radiocarbon from dispersed charcoal in the paleosol beneath it (e.g., Big Island in Hawaii, Rubin et al. 1987; Iceland, Hauptfleisch and Einarsson 2012; and Nicaragua, Avellán et al. 2023).

The resultant AMS ^{14}C ages from scattered charcoal within the paleosol's top portion covered by the studied lava flows help obtain the Masaya flank eruption's geochronological record. $\Delta^{14}C$ shows negative values that increase with ^{14}C ages (Table 2), which indicates that the dated paleosols have remained in a closed system isolated from the atmosphere, allowing radioactive decay (e.g., Trumbore et al. 2016), and thus providing reliable ages.

AMS ^{14}C dating of the paleosol sample beneath the Mosintepe lava flow provided an age of 2250 ± 30 years BP, corresponding to calendar age intervals on the calibration curve between 285–229 and 386-353 cal BC at 1σ (68.2% probability) (Table 2; Figure 5A). The highest probability range with confidence of up to 42.1% within 1σ of the *Mo* Unit overlaps the highest probability interval within 2σ (Figure 5A). The most likely calendar age of this eruption falls in the range of 285–229 cal BC. The *Mo* Unit is isolated from the other lava flows, without a direct stratigraphic relationship. However, we consider that the age for this eruption is consistent with its stratigraphic position because the underlying paleosol was developed from the Masaya Tuff, which was reported with an age of 3485 ± 90 years BP (Avellán et al. 2012).

https://doi.org/10.1017/RDC.2025.10143 Published online by Cambridge University Press

Table 3. *Geochemical analyses results for major and trace elements of the studied lava flow units*

Sample	C5	C4	C1	C3	C2	C6	C7
Unit	Mosintepe	Portillo	Gorgonia	Campuzano	Martha	Nindiri	Masaya
East coordinate	593405	592103	590738	593262	593802	590230	592627
North coordinate	1337998	1335236	1329855	1332744	1331696	1327302	1325857
Major elements (wt%)							
SiO_2	51.64	51.39	52	50.14	51.6	50.67	50.91
Al_2O_3	14.9	15.43	16.32	15.8	14.85	16.91	15.76
Fe_2O_3 [T]	13.34	13.22	11.84	12.99	13.79	12.57	13.45
MnO	0.221	0.22	0.202	0.214	0.231	0.209	0.227
MgO	5.64	5.75	5.01	5.71	5.26	4.83	5.22
CaO	9.93	10.06	10.14	9.71	9.77	10.35	9.9
Na_2O	2.74	2.82	2.81	2.78	2.74	2.61	2.7
K_2O	1.13	1.18	1.15	1.17	1.26	1.06	1.15
TiO_2	1.121	1.099	1.024	1.107	1.213	1.082	1.15
P_2O_5	0.25	0.24	0.23	0.25	0.27	0.25	0.25
LOI	–0.32	–0.57	–0.18	–0.35	–0.27	–0.34	–0.46
Total	100.6	100.8	100.6	99.51	100.7	100.2	100.3
Trace elements (ppm)							
Ba	843	852	818	839	908	816	876
Cs	0.8	0.8	0.8	0.8	0.9	0.8	0.8
Nb	2.5	2.6	2.3	2.2	2.6	2.7	2.9
Pb	5	5	5	5	5	5	6
Rb	22	22	22	22	24	20	22
Sr	425	444	466	451	417	458	437
Ta	0.15	0.16	0.15	0.13	0.15	0.13	0.13
Th	1.7	1.7	1.76	1.76	1.81	1.58	1.71
U	1.37	1.43	1.38	1.41	1.52	1.31	1.47
Y	21	23	21	20	23	23	24
Zr	90	92	84	83	96	82	89
La	10.6	10.4	10.4	10.7	11.5	9.42	10.4
Ce	22.6	22	22	23.3	24.1	19.6	21.7
Pr	3.31	3.2	3.17	3.33	3.53	3.13	3.4
Nd	15.5	14.7	14.6	15.1	16.6	15.3	16.3
Sm	4.11	3.89	3.77	4.05	4.28	4	4.34
Eu	1.22	1.22	1.18	1.27	1.33	1.22	1.28
Gd	4.2	4.09	4.09	4.27	4.7	3.81	4.01
Tb	0.66	0.69	0.65	0.67	0.73	0.61	0.69
Dy	4.31	4.18	3.96	4.23	4.66	3.91	3.99
Ho	0.86	0.85	0.83	0.86	0.94	0.79	0.85
Er	2.56	2.47	2.5	2.54	2.76	2.29	2.45
Tm	0.363	0.364	0.367	0.344	0.409	0.338	0.376
Yb	2.46	2.37	2.34	2.41	2.68	2.25	2.33
Lu	0.395	0.378	0.374	0.405	0.428	0.375	0.377

The age of the paleosol beneath the Portillo lava flow of 1610 ± 30 years BP provided calibrated age intervals of 496–534, 455–478, and 418–440 cal AD at 1σ (Table 2; Figure 5B); the first mentioned interval presents the highest reliability value with 31.4%, so we propose it as the calibrated age of this eruption (Table 2; Figure 5B). The age obtained for the *Po* Unit is consistent with its stratigraphic

https://doi.org/10.1017/RDC.2025.10143 Published online by Cambridge University Press

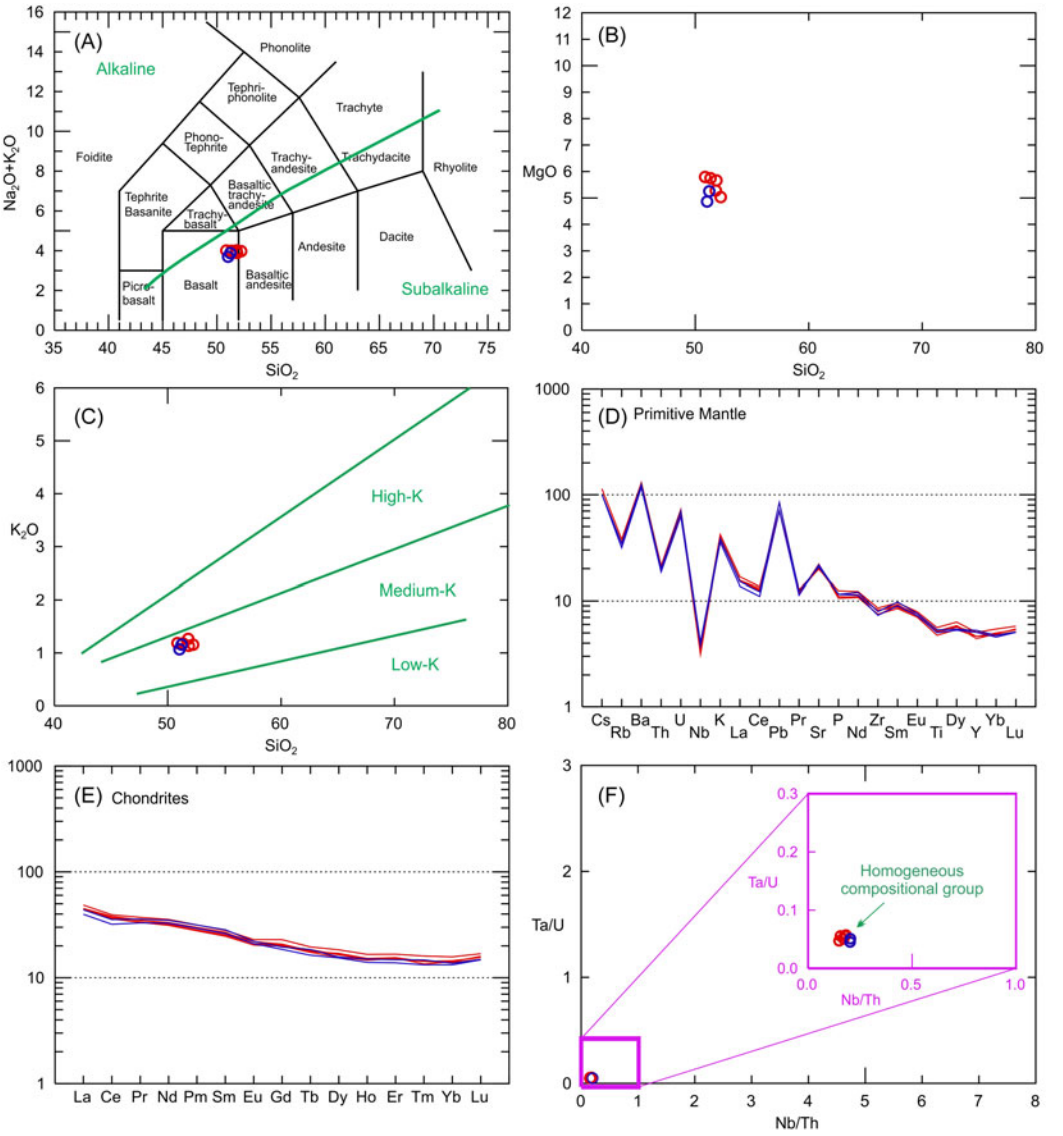

Figure 4. *Geochemical results for the studied lava flows. A, Total alkalis vs. silica diagram after Le Maitre et al. (1989). After Irvine and Baragar (1971), the green line divides alkaline and sub-alkaline rocks. B, MgO vs. SiO_2 Harker diagram. C, K_2O vs. SiO_2 Harker diagram after Gill (1981) showing that all the samples have medium-K content. D, Trace element plot normalized to primitive mantle from Sun and McDonough (1989). E, Multi-element plot comparing normalized rare earth elements to chondrite values in ppm from Sun and McDonough (1989). F, Ta/U vs. Nb/Th Harker diagram revealing a homogeneous compositional group. The red symbols represent the five studied lava flows in Masaya's northern rift zone (Mosintepe, Portillo, Gorgonia, Campuzano, and Martha), and the blue symbols represent the historical eruptions of 1670 (Upper Nindirí) and 1772 (Upper Masaya) CE within the Masaya caldera for comparison.*

position since it also overlies the Masaya Tuff eruption of 3.5 ka and is partially overlain by the younger Campuzano lava flow.

By examining the age of the paleosol beneath the Gorgonia lava flow of 1600 ± 30 years BP, it corresponds to calendar age intervals of 496–535, 449–478, and 425–441 cal AD in 1σ (Table 2; Figure 5C).

https://doi.org/10.1017/RDC.2025.10143 Published online by Cambridge University Press

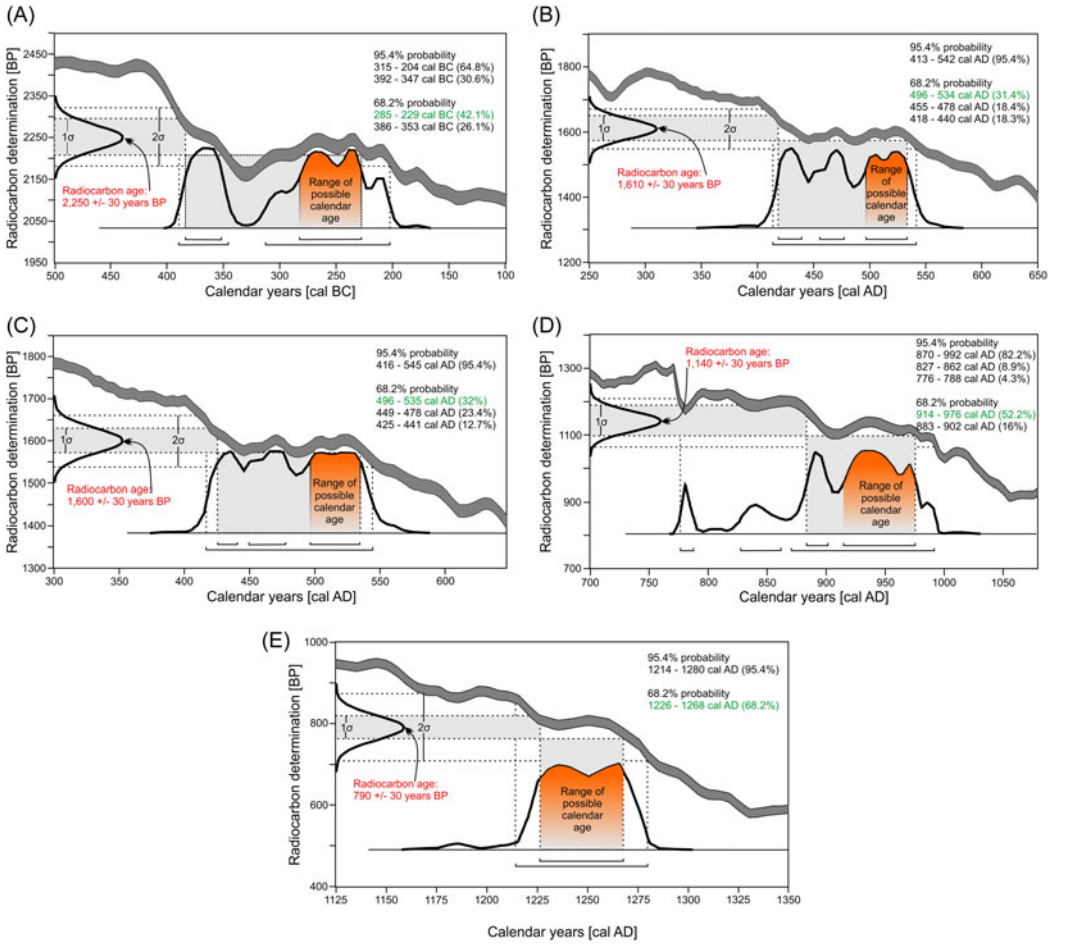

Figure 5. *Conventional and calibrated AMS ^{14}C dating results for the five studied lava flows. A, Age of the sample taken from the paleosol underlying the Mosintepe lava flow. B, Age from the paleosol underlying the Portillo lava flow; C, Age from the paleosol underlying the Gorgonia lava flow. D, Age from the paleosol underlying the Campuzano lava flow. E, Age from the paleosol underlying the Martha lava flow. The radiocarbon ages were calibrated to calendar years using IntCal20 (e.g., Ramsey 2009; Reimer et al. 2020).*

Considering the highest reliability with 32%, we propose the 496–535 cal AD interval as the age of the *Go* eruption. This unit is also isolated from the other units. However, the age is consistent with its stratigraphic position because it overlies the 3.5 ka Masaya Tuff. The *Go* eruption interval is equivalent to 496–535 cal AD, coinciding with the age range of the *Po* Unit, suggesting that these two lava flows could result from simultaneous eruptions, although not necessarily from the same eruption because the mapping reveals that they are spatially distinct fissural events.

The age of the paleosol beneath the Campuzano lava flow of 1140 ± 30 years BP produced calendar age intervals of 914–976 and 883–902 cal AD in 1σ (Table 2; Figure 5D). We propose that the youngest age interval of 914–976 cal AD is the calibrated age of the *Ca* Unit eruption, considering a 52.2% reliability. The radiometric age of this eruption is consistent with its stratigraphic position. In addition, this lava flow was located on the paleosol formed on the 3.5 ka Masaya Tuff deposit. The *Ca* Unit partially covers the 1.6 ka Portillo lava flow and is overlain by the younger Martha lava flow.

https://doi.org/10.1017/RDC.2025.10143 Published online by Cambridge University Press

The age of the paleosol underlying the Martha lava flow of 790 ± 30 years BP resulted in a calendar age interval of 1226–1268 cal AD in 1σ, presenting a simple distribution curve with a confidence value of up to 68.2% (Table 2; Figure 5E). Thus, we consider that this age range corresponds to the calibrated age of the eruption. The radiometric age obtained for this eruption is consistent with its stratigraphic position because the *Ma* lava flow is overlying the *Ca* Unit and is partially covered by the 1772 lava flow that occurred on the flank of the post-caldera Masaya volcano.

Volcanic provenance

It was determined that at least five lava flows occurred on the northern flank of the Masaya caldera parallel to the Cofradía fault zone (Figure 2), with eruptive centers located 0.7 to 8.2 km from the caldera's fault rim. The eruptive vents built small spatter cones linked to different lava flow units, each recognized as an independent eruption. Surface geological mapping suggests that these lava flows may correspond to monogenetic volcanoes sourced by independent magma feeder dikes (e.g., Gómez-Vasconcelos et al. 2023). However, after chemical examination of major and trace elements, it is suggested that magmas share a common provenance.

Rocks collected from Masaya's northern flank and the 1670 and 1772 historical eruptions within the caldera show almost identical lithological and petrographical characteristics (Figure 4). All rocks are gray, fine-grained, and porphyritic with plagioclase (55–47 vol%), pyroxene (45–29 vol%), olivine (11–5 vol%), and Fe-Ti oxides (5–1.7 vol%). All lava flow units have a very narrow range in composition, from dominantly silica-rich basalt to basaltic andesite (50.14–52.00 wt% SiO_2) (Figure 4A). They also present similar MgO content with values between 4.83 and 5.75 wt% (Figure 4B; Table 3), and medium-K_2O content between 1.07 and 1.27 wt% (Figure 4C; Table 3). On the other hand, selected high-field strength trace elements also reveal a homogeneous compositional group (Nb/Th-Ta/U) (e.g., Avellán et al. 2024; Gómez-Vasconcelos et al. 2020) (Figure 4F). This suggests that the post-caldera basaltic effusive eruptions that occurred on the northern flank of the Masaya caldera are comagmatic with the historical eruptions that occurred in 1670 and 1772 CE within the caldera (Figure 2). In addition, the concentrations of trace elements reveal that all lava flows show identical behavior to the historical eruptions within the caldera (Figures 4D and 4E). This indicates that all these flank eruptions were affected by similar magmatic processes before reaching the surface and evidences a common geochemical fingerprint (e.g., Casadevall and Dzurisin 1987). Therefore, these similar characteristics suggest that Masaya's northern flank eruptions are independent structures that originated from the same magma chamber that feeds Masaya caldera (Figure 6).

This suggests that magma propagated laterally from Masaya's central magma system (Figure 6) controlled by a local compressional stress field due to the surface load of the large caldera. It is believed that this compressional stress impedes effusive, volatile-poor, dense magmas from reaching the surface; thus, they can only propagate laterally on the volcano's slopes (e.g., Gudmundsson 2020; Pinel and Jaupart 2004). Therefore, post-caldera volatile-poor magmas in Masaya will likely propagate horizontally to feed a distal flank vent (up to 13 km from the summit crater). Flank eruptions here migrate north because the N–S Aeropuerto graben and associated bounding faults (i.e., Cofradía fault; Figure 2) represent Masaya's local volcanic rift zone, and this crustal transtensional weakness assists magma emplacement (Girard and de Vries 2005). Furthermore, this study reveals that flank eruptions are recurrent in the Masaya caldera along the northern volcanic rift zone.

Kilauea and Mauna Loa volcanoes present well-documented examples of flank eruptions in their geological record (Holcomb 1987; Lockwood and Lipman 1987; Lockwood et al. 1987; Tilling et al. 1987; Wolfe et al. 1987). Flank eruptions linked to local rift zones are also common in Piton de la Fournaise (Peltier et al. 2005), Ambryn (Németh and Cronin 2008), Nyiragongo (Komorowski 2002), Fjallgardar in Iceland (Löw et al. 2025) and Etna volcanoes (Acocella and Neri 2003). Flank eruptions from these volcanoes report lateral dike propagation from the volcano summit over great distances, up to 100 km, although mean flank eruptions are found within the first 20 km from the summit crater (Löw et al. 2025; Patrick et al. 2020).

https://doi.org/10.1017/RDC.2025.10143 Published online by Cambridge University Press

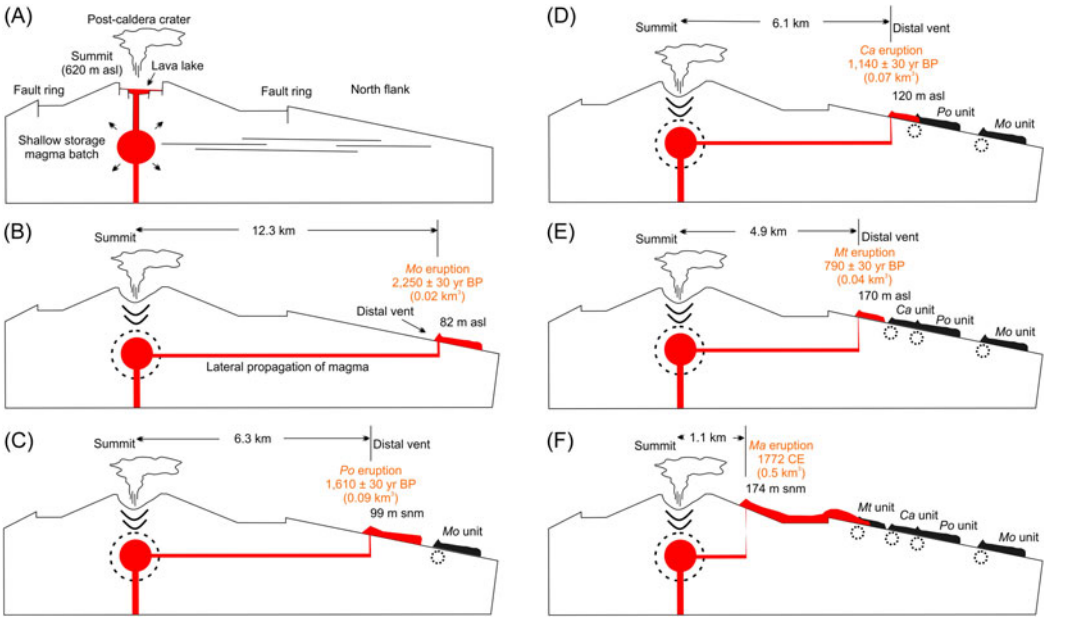

Figure 6. *Sketch model for Masaya's lateral magma propagation from the central magma batch to the northern flank to feed Mosintepe, Portillo, Gogonia, Campuzano, and Martha lava flows.*

As these studied eruptions show a similarity in mineral paragenesis, behavior of trace element concentrations, and K content, it reveals that the magmas were stored in the same shallow magma chamber and cannot be considered as monogenetic volcanoes. A monogenetic volcano would show a rapid ascent from the deep crust, thus a less differentiated magma with depletion in K content (e.g., primitive or tholeiitic magma; Avellán et al. 2012) and less fractionated rare earth elements.

Regional geochronological context

The new AMS ^{14}C ages reveal Masaya's frequent effusive activity during the Holocene. The *Mo* eruption happened on the northern flank of the Masaya caldera in the mid-3rd century BC, emitting a bulk volume of 0.02 km^3 (Figures 2 and 6B). Later, two other eruptions (*Po* and *Go* Units) took place in the late 5th and early 6th century AD, emitting a bulk volume of 0.09 and 0.04 km^3, respectively (Figures 2 and 6C). Afterward, another eruption occurred in the mid-10th century AD (*Ca* Unit), emitting a bulk volume of 0.07 km^3 (Figures 2 and 6D). Then, the *Ma* Unit occurred in the mid-13th century AD and emitted a bulk volume of 0.04 km^3 (Figures 2 and 6E). All these eruptions happened during the pre-Hispanic period (Figure 7).

At the beginning of the colonial period, the Masaya caldera developed a shallow lava lake in the Nindirí post-caldera crater (Fernández de Oviedo 1851) (Figure 2). The Santiago and San Pedro post-caldera pit craters formed at the caldera's summit, sourcing lava lakes (Harris 2009; Rymer et al. 1998). Historic effusive eruptions include the one from the Nindirí crater in 1670 CE (Figure 7) that emplaced a 2.4 km-long lava flow with 0.1 km^3 of emitted bulk volume. The last recorded eruption was the one from the Masaya post-caldera crater in 1772 CE. This lava flow emitted a minimum bulk volume of 0.51 km^3 and reached 7.9 km to the north, surpassing the caldera's ring fault border and partially covering *Mt* Unit (Table 1; Figures 2 and 6F).

Although the geological record is still poorly established, this work reveals that the Masaya caldera is an active volcanic system and is currently dominantly effusive. Up to nine eruptions have been recorded

https://doi.org/10.1017/RDC.2025.10143 Published online by Cambridge University Press

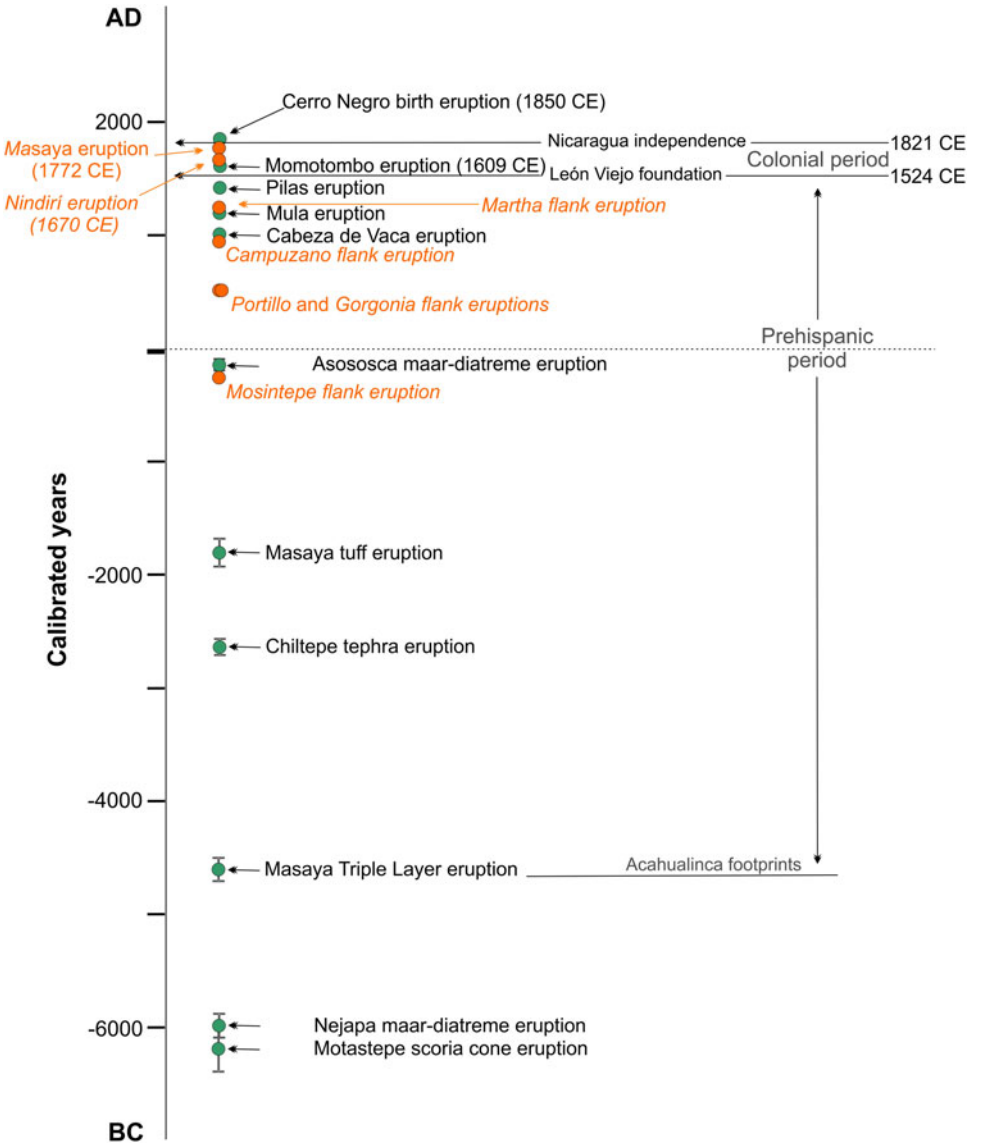

Figure 7. *Graphical representation showing Masaya's eruptions and the stratigraphic relationship with other documented Holocene eruptions in the Nicaraguan Volcanic Arc.*

during the Holocene. Two explosive eruptions, the Masaya Tuff and the Masaya Triple Layer, occurred at 3.485 ± 90 and 5755 ± 90 years BP, respectively (Avellán et al. 2012) (Figures 3 and 7), and seven effusive eruptions, including five flank eruptions (studied here) and the historical 1670 and 1772 CE eruptions. This results in an average recurrence rate of 1.45×10^{-3} eruptions/year for the last 5.7 ka, equivalent to a return period of 633 years. For effusive flank eruptions, the average recurrence rate is 2.5×10^{-3} eruptions/year for the last 2.25 ka, equivalent to a return period of 375 years, which is twice as often. However, these values should be handled carefully because the Masaya caldera geological record of effusive eruptions remains incomplete.

Flank eruptions are also geochronologically interspersed with other regional eruptions. Like the one that occurred in the Nejapa volcanic field with a radiometric age of 2130 ± 40 years BP (Avellán et al.

https://doi.org/10.1017/RDC.2025.10143 Published online by Cambridge University Press

2012), which is younger than the Mosintepe eruption and older than the Portillo, Gorgonia, and Campuzano eruptions (Figure 7). While the Martha eruption is interspersed with monogenetic Mula and Pilas eruptions that occurred north of the Cerro Negro volcano (Figure 7).

Conclusions

This study reports five new flank eruptions in the northern rift zone of the Masaya caldera within the N–S Aeropuerto graben and parallel to the Cofradía fault zone. These eruptions comprise effusive and basaltic lava flows up to 8 km long from their vent, releasing a total bulk volume of 0.26 km^3. Radiocarbon AMS dates are 285–229 cal BC for Mosintepe, 496–534 cal AD for Portillo, 496–535 cal AD for Gorgonia, 914–976 cal AD for Campuzano, and 1226–1268 cal AD for Martha. Geochemistry reveals that these magmas have a common origin with the Masaya caldera, suggesting that lateral magma draining happens frequently from a shallow magma batch.

The active Masaya caldera is primarily effusive, where flank eruptions happen every ca. 375 years. Therefore, future effusive flank eruptions will likely develop in its northern rift zone, putting downward-sloping localities like Veracruz, Cofradía, Sabana Grande, eastern Managua, and new settlements at risk. Urban growth should be regulated to avoid future impacts in this area, and these eruptions should be considered to complete the caldera's geological record for a better hazard and risk assessment.

Acknowledgments. This work is dedicated to the memory of geologists Glen Hodgson, Alberto Pilato, Antonio Alvarez, Mario Chavez, Mayra Guerrero, and Ricardo López. Special thanks to N. Castillo for his valuable support during fieldwork. We also thank N. Fitz for his help in data processing, and thanks to J.A. Gómez for her support in the preparation of the thin sections. We thank A.J.T. Jull, K. Németh, and H. Murcia for their valuable reviews that helped improve the manuscript.

Declaration of competing interests. The authors declare no conflicts or competing interests.

References

Acocella V and Neri M (2003) What makes flank eruptions? The 2001 Etna eruption and its possible triggering mechanisms. *Bulletin of Volcanology* **65**, 517–529. https://doi.org/10.1007/s00445-003-0280-3

Actlabs (2025) https://actlabs.com/

Avellán DR, Cardona-Melchor S, Gómez-Vasconcelos MG, Macías JL, Layer PW, Sosa-Ceballos G, Ruíz MC, Benowitz J, Cisneros-Máximo G, Murcia H, Perthon M, Reyes-Agustín G and García-Tenorio F (2024) The Nieve volcanic cluster: A Pliocene-Pleistocene lava dome cluster in the Michoacán-Guanajuato volcanic field (México). *Journal of Volcanology and Geothermal Research* **450**, 108091. https://doi.org/10.1016/j.jvolgeores.2024.108091

Avellán DR, Gómez-Vasconcelos MG, Macías JL and Velásquez G (2023) AMS ^{14}C ages determination of the late Holocene Pilas, Mula and Cabeza de Vaca monogenetic volcanoes, Nicaragua. *Journal of South American Earth Sciences* **123**, 104194. https://doi.org/10.1016/j.jsames.2023.104194

Avellán DR, Macías JL, Pardo N, Scolamacchia T and Rodriguez D (2012) Stratigraphy, geomorphology, geochemistry and hazard implications of the Nejapa Volcanic Field, western Managua, Nicaragua. *Journal of Volcanology and Geothermal Research* **213**, 51–71. https://doi.org/10.1016/j.jvolgeores.2011.11.002

Beta Analytic (2025) https://www.radiocarbon.com/

Casadeval TJ and Dzurisin D (1987) Stratigraphy and petrology of the Uwekahuna bluff section, Kilauea caldera. Volcanism in Hawaii. *Geological Survey Professional Paper* **1350**(1), 351–375.

Dieterich JH (1988) Growth and persistence of Hawaiian volcanic rift zones. *Journal of Geophysical Research: Solid Earth* **93**(B5), 4258–4270. https://doi.org/10.1029/JB093iB05p04258

Fernández de Oviedo G (1851) Historia general y natural de las indias, islas y tierra firme del mar océano, primera parte. *Real Academia de Historia.*

Gill JB (1981) *Orogenic Andesite and Plate Tectonics*. Springer.

Girard G and de Vries BVW (2005) The Managua Graben and Las Sierras-Masaya volcanic complex (Nicaragua); pull-apart localization by an intrusive complex: Results from analogue modeling. *Journal of Volcanology and Geothermal Research* **144**(1–4), 37–57. https://doi.org/10.1016/j.jvolgeores.2004.11.016

Global Volcanism Program (2024) Available at: https://volcano.si.edu/volcano.cfm?vn=344100

Gómez-Vasconcelos MG, Macías JL, Avellán DR, Sosa-Ceballos G, Garduño-Monroy VH, Cisneros-Máximo G, Layer PW, Benowitz J, López-Loera H, Mendiola-López F and Perton M (2020) The control of preexisting faults on the distribution, morphology, and volume of monogenetic volcanism in the Michoacán-Guanajuato volcanic field. *GSA Bulletin* **132**(11/12), 2455–2474. https://doi.org/10.1130/B35397.1

https://doi.org/10.1017/RDC.2025.10143 Published online by Cambridge University Press

Gómez-Vasconcelos MG, Avellán DR, Macías JL, Cisneros-Máximo G, Sánchez-Núñez JM and Miggins DP (2023) New insights into feeder dike swarms in scoria cones and their structural control: A case study in the Michoacán-Guanajuato volcanic field. *Geology Today* **33**(2), 3–10. https://doi.org/10.1130/GSATG539A.1

Gudmundsson A (2020) *Volcanotectonics: Understanding the Structure, Deformation and Dynamics of Volcanoes*. Cambridge University Press.

Gudmundsson A and Loetveit IF (2005) Dyke emplacement in a layered and faulted rift zone. *Journal of Volcanology and Geothermal Research* **144**(1–4), 311–327. https://doi.org/10.1016/j.jvolgeores.2004.11.027

Harris AJ (2009) The pit-craters and pit-crater-filling lavas of Masaya volcano. *Bulletin of Volcanology* **71**, 541–558. https://doi.org/10.1007/s00445-008-0241-y

Hauptfleisch U and Einarsson Á (2012) Age of the younger Laxá lava and lake Mývatn, northern Iceland, determined by AMS radiocarbon dating. *Radiocarbon* **54**(2), 155–164. http://dx.doi.org/10.2458/azu_js_rc.v54i2.15970

Holcomb RT (1987) Eruptive history and long-term behavior of Kilauea volcano. Volcanism in Hawaii. *Geological Survey Professional Paper* **1350**(1), 261–350.

Irvine TNJ and Baragar WRA (1971) A guide to the chemical classification of the common volcanic rocks. *Canadian Journal of Earth Sciences* **8**(5), 523–548. https://doi.org/10.1139/e71-055

Kaneko T, Yasuda A, Shimano T, Nakada S, Fujii T, Kanazawa T, Nishizawa A and Matsumoto Y (2005) Submarine flank eruption preceding caldera subsidence during the 2000 eruption of Miyakejima Volcano, Japan. *Bulletin of Volcanology* **67**, 243–253. https://doi.org/10.1007/s00445-004-0407-1

Komorowski JC (2002) The January 2002 eruption-The January 2002 flank eruption of Nyiragongo Volcano (Democratic Republic of Congo): Chronology, evidence for a tectonic rift trigger, and impact of lava flows on the city of Goma. *Acta Vulcanologica: Journal of the National Volcanic Group of Italy* **14/15**(1/2), 1000–1035.

Kutterolf S, Freundt A, Perez W, Wehrmann H and Schmincke HU (2007) Late Pleistocene to Holocene temporal succession and magnitudes of highly-explosive volcanic eruptions in west-central Nicaragua. *Journal of Volcanology and Geothermal Research* **163**(1–4), 55–82. https://doi.org/10.1016/j.jvolgeores.2007.02.006

La Femina PC, Dixon TH and Strauch W (2002) Bookshelf faulting in Nicaragua. *Geology* **30**(8), 751–754. https://doi.org/10.1130/0091-7613(2002)030%3C0751:BFIN%3E2.0.CO;2

Le Maitre RW (1989) A classification of igneous rocks and glossary of terms: Recommendations of the international union of geological sciences subcommission on the systematics of igneous rocks.

Lockwood JP, Dvorak JJ, English TT, Koyanagi RY, Okamura AT, Summers ML and Tanigawa WR (1987) Mauna Loa 1974–1984: A decade of intrusive and extrusive activity. Volcanism in Hawaii. *Geological Survey Professional Paper* **1350**(1), 537–570.

Lockwood JP and Lipman PW (1987) Holocene eruptive history of Mauna Loa volcano. Volcanism in Hawaii. *Geological Survey Professional Paper* **1350**(1), 509–535.

Löw N, Halldórsson SA, Beier C, Bali E, Matthews S, Guðfinnsson GH, Marshall EW, Helgason J, Ranta E, Abersteiner A, Barnes JD and Caracciolo A (2025) Magma storage and transport beneath the near-rift Fjallgarðar Volcanic Ridge, Northeast Iceland. *Contributions to Mineralogy and Petrology* **180**(3), 1–25. https://doi.org/10.1007/s00410-025-02212-w

McBirney AR (1956) The Nicaraguan volcano Masaya and its caldera. *Eos, Transactions American Geophysical Union* **37**(1), 83–96. https://doi.org/10.1029/TR037i001p00083

Moore JG and Clague DA (1992) Volcano growth and evolution of the island of Hawaii. *Geological Society of America Bulletin* **104**(11), 1471–1484. https://doi.org/10.1130/0016-7606(1992)104%3C1471:VGAEOT%3E2.3.CO;2

Németh K and Cronin SJ (2008) Volcanic craters, pit craters and high-level magma-feeding systems of a mafic island-arc volcano: Ambrym, Vanuatu, South Pacific. *Geological Society, Special Publications* **302**, 153–176. https://doi.org/10.1144/SP302.6

Patrick MR, Houghton BF, Anderson KR, Poland MP, Montgomery-Brown E, Johanson I, Thelen W and Elias T (2020) The cascading origin of the 2018 Kīlauea eruption and implications for future forecasting. *Nature Communications* **11**(1), 5646. https://doi.org/10.1038/s41467-020-19190-1

Peltier A, Ferrazzini V, Staudacher T and Bachèlery P (2005) Imaging the dynamics of dyke propagation prior to the 2000–2003 flank eruptions at Piton de La Fournaise, Reunion Island. *Geophysical Research Letters* **32**(22). https://doi.org/10.1029/2005GL023720

Pinel V and Jaupart C (2004) Likelihood of basaltic eruptions as a function of volatile content and volcanic edifice size. *Journal of Volcanology and Geothermal Research* **137**(1–3), 201–217. https://doi.org/10.1016/j.jvolgeores.2004.05.010

Ramsey CB (2009) Bayesian analysis of radiocarbon dates. *Radiocarbon* **51**(1), 337–360.

Reimer PJ (2020) Composition and consequences of the IntCal20 radiocarbon calibration curve. *Quaternary Research* **96**, 22–27. https://doi.org/10.1017/S0033822200033865

Rubin M, Gargulinski LK and McGeehin JP (1987) Hawaiian radiocarbon dates. Volcanism in Hawaii. *Geological Survey Professional Paper* 1350(1), 213–242.

Rymer H, van Wyk de Vries B, Stix J and Williams-Jones G (1998) Pit crater structure and processes governing persistent activity at Masaya Volcano, Nicaragua. *Bulletin of Volcanology* **59**, 345–355. https://doi.org/10.1007/s004450050196

Simkin T and Howard KA (1970) Caldera collapse in the Galápagos Islands, 1968: The largest known collapse since 1912 followed a flank eruption and explosive volcanism within the caldera. *Science* **169**(3944), 429–437. https://doi.org/10.1126/science.169.3944.429

https://doi.org/10.1017/RDC.2025.10143 Published online by Cambridge University Press

Sun SS and McDonough WF (1989) Chemical and isotopic systematics of oceanic basalts: Implications for mantle composition and processes. *Geological Society, London, Special Publications* **42**(1), 313–345. https://doi.org/10.1144/GSL.SP.1989.042.01.19

Tilling RI, Christiansen RL, Duffield WA, Endo ET, Holcomb RT, Koyanagi RY, Peterson DW and Unger JD (1987) The 1972–1974 Mauna Ulu eruption, Kilauea volcano: An example of quasi-steady-state magma transfer. Volcanism in Hawaii. *Geological Survey Professional Paper* **1350**(1), 405–469.

Trumbore SE, Sierra CA and Hicks-Pries CE (2016) Radiocarbon nomenclature, theory, models, and interpretation: Measuring age, determining cycling rates, and tracing source pools. In Schuur E, Druffel E and Trumbore S (eds), *Radiocarbon and Climate Change: Mechanisms, Applications and Laboratory Techniques*. Springer, 45–82. https://doi.org/10.1007/978-3-319-25643-6_3

Wolfe EW, Garcia MO, Jackson DB, Koyanagi RY, Neal CA and Okamura AT (1987) The Puu oo eruption of Kilauea volcano, episodes 1–20, January 3, 1983, to June 8, 1984. Volcanism in Hawaii. *Geological Survey Professional Paper* **1350**(1), 471–508.

Xu S, Hoshizumi H, Uto K and Freeman SPH (2013) Radiocarbon dating of Fugendake volcano in Unzen, SW Japan. *Radiocarbon* **55**(2–3), 1850–1861. https://doi.org/10.1017/S0033822200048761

Cite this article: Avellán D-R, Gómez-Vasconcelos MG, and Pilato M. Holocene effusive flank eruptions in Masaya caldera, Nicaragua. *Radiocarbon* 1–17. https://doi.org/10.1017/RDC.2025.10143